# Molecular imaging of biological samples with sub-cellular spatial resolution and high sensitivity

Marvin Vestal, Christina Vestal, Sicheng Li, Kenneth Parker
SimulTOF Systems

**Introduction**

Imaging mass spectrometry is a mature technology that produces ion maps or images from the direct desorption of molecules from cells in tissues.[1] Spatial resolutions of about 20 μm can be achieved routinely by standard commercial instruments.[2] Recent work employing matrix deposition by sublimation and rehydration has produced protein images with 10 μm spatial resolution in favorable cases, such as the islets of Langerhans in pancreas, but speed and sensitivity are inadequate for many practical applications. [3-5] A new MALDI-TOF imaging system that provides very high acquisition rates, high spatial resolution, and efficient ionization and detection has recently been developed.[6,7] Here we demonstrate high performance for imaging lipids at 20 μm spatial resolution using a laser beam with effective diameter less than 5 μm. In this work we sublimated DAN matrix using established protocols and found that spatial resolution in this case, at least down to 5 μm, is not limited by size of the crystals.

The MALDI-TOF mass spectrometer employs a new ion optics system that provides very high sensitivity, precision, and dynamic range for both positive and negative ions over a broad mass range. [8-10] The instrument includes a solid-state Nd:YLF laser that provides 349 nm photons with fluence up to 30 μJ at 5kHz. The effective laser spot diameter is adjustable from 5 to 30 μm under computer control. A new 8 Bit High Speed Digitizer with an ADC sampling rate up to 2.5 GS/s on a single channel is employed.

We have demonstrated the ability to acquire and save single-shot spectra at a rate of 5000/s, but for many applications the effective speed is limited by the time required to process the large files generated from spectra covering a broad mass range. At present the maximum rate for processing and transferring to disk the files generated for lipid imaging is about 750 pixels/s. The 5 kHz laser allows averaging 5 laser pulses/pixel at acquisition rate of 1000 pixels/s or 10 laser pulses/pixel at acquisition rate of 500 pixels/s. The effective rates, including data transfer, are then 430 and 300 pixels/s for these two cases. In general, increasing the number of laser shots per pixel increases the dynamic range by providing more ions detected per pixel. In this work we provide quantitative data on the tradeoff between speed and dynamic range for imaging of lipids.

**Instrument Performance**

Our focus in this work is on instrument performance, but we recognize that sample preparation and matrix application are essential. For this we have depended on our colleagues who are recognized leaders in all aspects of IMS. [11-13] Successful completion of our present work was dependent on the quality of the samples and the matrix application.

A recent excellent review by Schulz et al [14] defines the '4S criteria for performance in MSI. "The ideal mass spectrometer for MALDI MSI would satisfy the '4S-criteria for performance (Speed, Specificity, Spatial Resolution, and Sensitivity). However, increases in spatial resolution will invariably lead to smaller ablation areas and thus limit sensitivity; and need for speed must be balanced against the other three criteria." No one is likely to dispute the importance of these four criteria, but we propose adding 3 more, namely: Stability, Simplicity, and Size (of sample and data files). Also, our results show that higher spatial resolution does not invariably limit sensitivity, since the decrease in ablation area may be overcome by higher ionization and detection efficiency for the molecules irradiated. Our goal in this work is to evaluate the MALDI-TOF instrument described here toward satisfying all '7S criteria' for the ideal MSI mass spectrometer. The linear analyzer provides maximum resolving power of 4000 and routine mass accuracy +/-0.1Da; this provides adequate specificity for many applications, but cannot distinguish many of the large number of lipid structures that occur.

We chose pancreas for our initial applications [6] since it was known that the alpha and beta cells in the islets of Langerhans are marked by high levels of glucagon and insulin respectively, so it might be possible to detect single cells.[15] We were supplied the samples with no info except that they were mouse pancreas prepared for imaging of proteins. When we received the samples our first reaction was "This an awfully big mouse" It turned out to be rat. The goal was to image these at 10 μm spatial resolution and find and characterize the islets of Langerhans for obese, lean and diabetic rat. Recently we have obtained some images of mouse pancreas islets at 5 μm spatial resolution, but have not yet improved our ability to detect proteins from single cells. The problem with protein imaging is primarily concerned with sample preparation and matrix deposition, and that work is continuing.

**Images of lipids in rat brain**

Recent published work has shown that lipid profiles in brain showed a more complicated structure than other tissues examined, and negative ion images often provided more high resolution detail than the positive ion images. [16-18]This earlier work demonstrated the ability to obtain excellent images of rat and mouse brain sections with 20 μm spatial resolution at a rate of 20 pixels/s. Since we had already demonstrated higher speed and higher resolution on proteins in pancreas samples, this appeared to provide a more definitive test of our new MALDI-TOF imaging instrument. The samples were provided by Jeff Spraggins mounted on ITO glass slides with sublimated DAN matrix applied. The sample plates were shipped at "dry ice" temperature and were kept in dry ice until they were thawed and loaded into the instrument. Spectra were acquired and images generated for both positive and negative lipid ions; but the negative ion images showed substantially more detailed structure and the data summarized here is limited to negative ions. Additional results for both negative and positive ions are available in Supplementary Material.

**Data acquisition and storage**

Mass spectral data were acquired with digitizer full scale at 1 volt and bin width of 1.6 ns. Spectra produced by 10 laser shots were summed, averaged, and recorded. Detector gain was adjusted so that the average response to a single ion was approximately $1x10^{-11}$ volt seconds (0.01 voltsx$1x10^{-9}$ s). Laser beam was 5 μm effective diameter operated at 5kHz, 5 μJ laser fluence with 10x attenuator delivering 0.5 μJ to sample. Spectra were acquired at 500 pixels/s with 10 laser shots/pixel corresponding to an effective rate of 300 pixels/s including data processing and saving to disk. Mass range was 300-1200 Da with 3000 mass resolution, mass error less than +/- 0.1 Da mass accuracy and all spectra acquired were saved.

**Examples of negative ion images of lipids in rat brain.**

One of the plates provided had 3 adjacent 10 μm thick sections, and these were used to evaluate performance at 20, 10, and 5 μm spatial resolution using sublimated 1,5-diaminonaphthalene (DAN) matrix for negative ions. The images shown in Figure 1 were acquired in 1 day starting at about 10 am and acquisition completed shortly after midnight. These runs were queued up to run automatically and the first 5 μm section started shortly before everyone left for the day. A program entitled "Analyze Masses" was also run automatically on all of the image data acquired. This program reformats the data in preparation for generating and viewing images, and typically takes less than one-half the time required to acquire the data. After this is completed, images of selected masses can be generated in a

few minutes even for files as large as 4 million pixels. Thus, the next morning we could start producing images, and the images shown in Figure 1 were finished in one day. The plate was left under vacuum until morning.

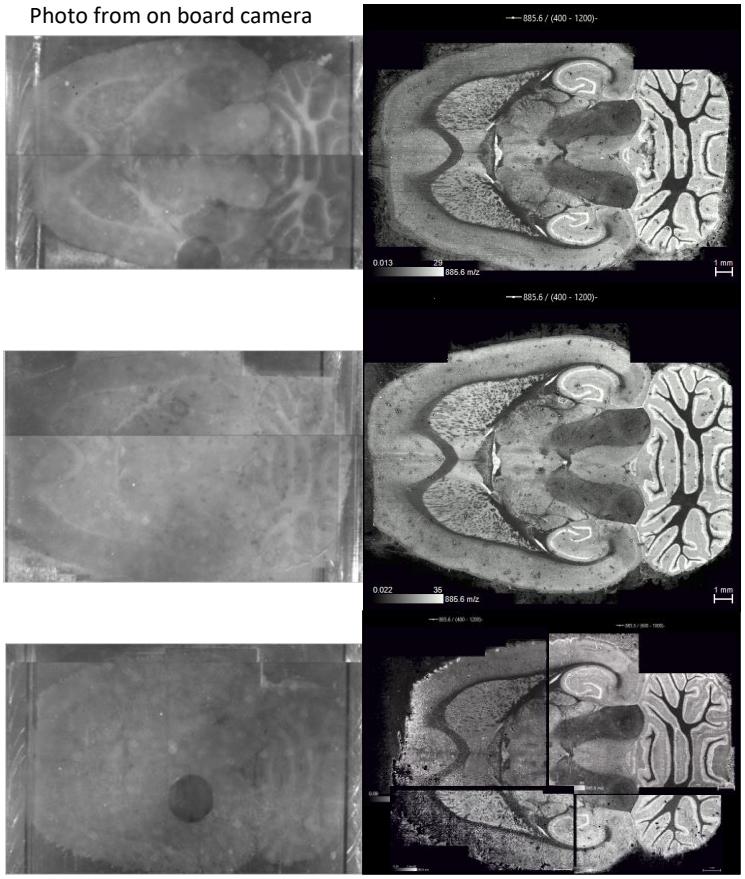


***This plate contained 3 serial sections of rat brain each about 3 cm$^2$ in area.***
All were imaged in one day using 5 kHz laser with 5um diameter laser, with net rate of 300 pixels/s at 10 shots/pixel.
**First segment**
**20** μm spatial resolution, with horizontal motion of **10** mm/s
659,519 pixels saved in 39 min, 6% of sample used
**Second segment**
**10** μm spatial resolution, with horizontal motion of **5** mm/s
2,813,271 pixels saved in 2 hr 48 min, 25% of sample used

**Third segment**
**5** μm spatial resolution, with horizontal motion of **2.5** mm/s
Split into 4 sections:
First section 3,691,614 pixels saved in 3 hr 10 min
Second section 3,515,258 pixels saved in 2 hr 54 min
Third section 1,767,795 pixels saved in 1 hr 28 min
Fourth section 1,486,208 pixels saved in 1 hr 18 min

10,460,875 pixels saved in 8 hr 50 min, 100% of sample used

**Total time: 12 hours and 7 minutes**
**Total Pixels: 14,000,000**
**140 million laser shots**

Figure 1. Negative ion Images of m/z 585.6 for three consecutive horizontal sections of mouse brain acquired at 20, 10, and 5 μm spatial resolution, respectively.

Inspecting the plate after ejecting from the instrument we saw that the DAN matrix was no longer visible even on portions not hit by the laser. The photo from the on-board camera taken after the run is shown on the left side of Figure 1. The photo of the first segment in which only 6% of the sample was removed is not noticeably different than original, but the third segment where essentially all of the sample was removed shows almost none of the sample structure. It may not be obvious from these images, but the dynamic range of the first part of the 5 μm image was similar to those at 10 and 20 μm spatial resolution, but the dynamic range in the other parts was somewhat reduced. The DAN matrix deposition appeared somewhat thinner than we sometimes observed, and it appears that a significant amount was vaporized after about 12 hours in vacuum.

It should be noted that using a laser beam with 5 um effective diameter the sensitivity with 5 μm spatial resolution is not less than that for 10 or 20 μm resolution. Summing over 16 5 μm-pixels to achieve 20 μm spatial resolution produces substantially higher ion yield than using a 20 μm diameter laser beam; the down side is that the 5 μm images takes 16 times longer to generate and produce a data file 16x larger. This can yield substantially higher sensitivity; but is not required for lipid imaging where the sample concentrations are relatively high. A more detailed quantitative study of ionization and detection efficiency dependence on laser spot diameter and laser fluence is outside the scope of the present work, but we have observed that, at least for lipids with DAN matrix, the ionization efficiency with the 5 μm laser beam is substantially higher than with a 20 μm diameter laser beam.

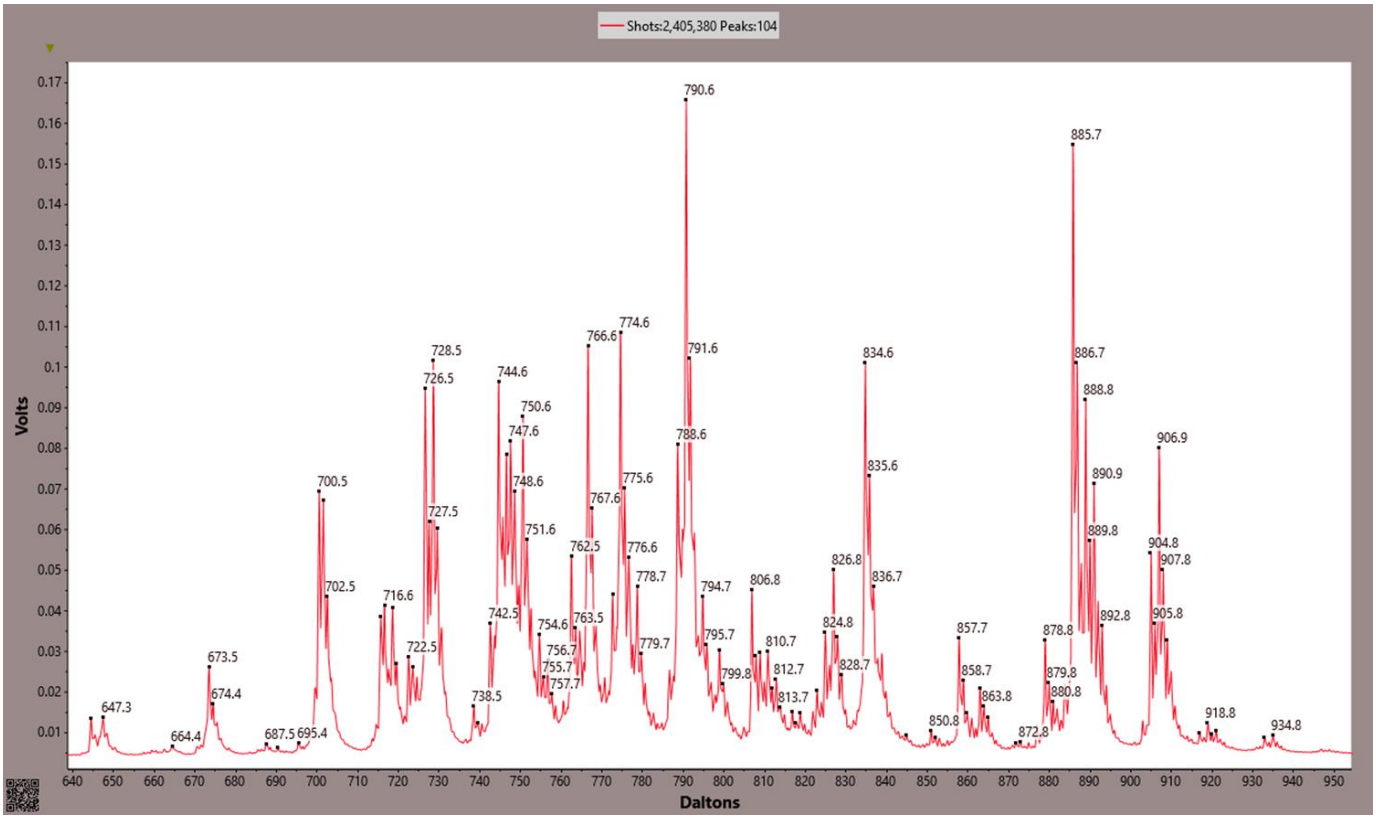


Figure 2. The spectrum obtained by summing over the full 10 um image in Figure 1 is shown.

This spectrum comprises 2,405,390 pixels with 10 laser shots/pixel. The intensities are calculated using a value of $10^{-11}$ volt seconds for the signal from a single ion that was determined by direct measurement of the average res.ponse for single ions. These data were acquired using a digitizer bin width of 1.6 ns, and the total number of ions per peak obtained by integrating over the peak is

typically about 3-4 times the peak intensity for these spectra. In this example there are 104 peaks in the mass range between m/z 600 and 950 with sufficient intensity to provide useful images and the total intensity is 38 billion ions corresponding to an average of 15,200 ions/pixel or 1520 ions/laser shot. The minimum intensity for the labeled peaks in Figure 2 is 1 million ions.

The spectrum from a single pixel selected at random from the image is shown in Figure 3. This spectrum is generated by summing 10 laser shots and each labelled peak comprises at least 10 ions detected. Many of the intense peaks in this spectrum are similar in intensity to those from the integrated spectrum, but it should be noted that several intense peaks in the integrated spectrum are absent from this pixel including nominal masses 878, 888, 890, 904, and 906 that appear to be signature ions for “white” matter in mouse and rat brain.

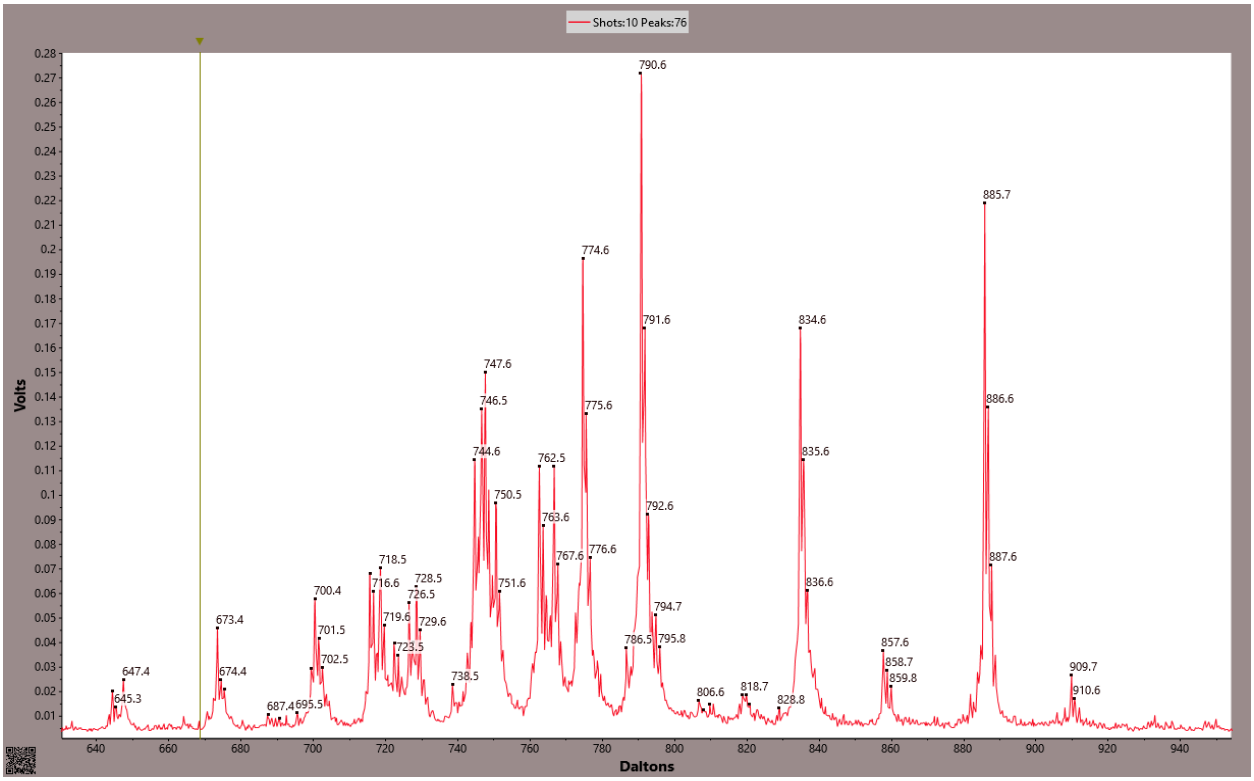


Figure 3 shows the mass spectrum from a single pixel chosen at random.

We have generated images of 25 masses selected from the list of 104 labelled in Figure 2, and the images of many of these are similar to others, but not identical. A gross separation appears to be “white” matter versus “gray” matter. An example of complimentary images is shown in Figure 4. Another example of comparison of the image of m/z 885.6 representing “gray” matter with the image of m/z 726.6 found almost exclusively in “white” matter is shown in Figure 5.

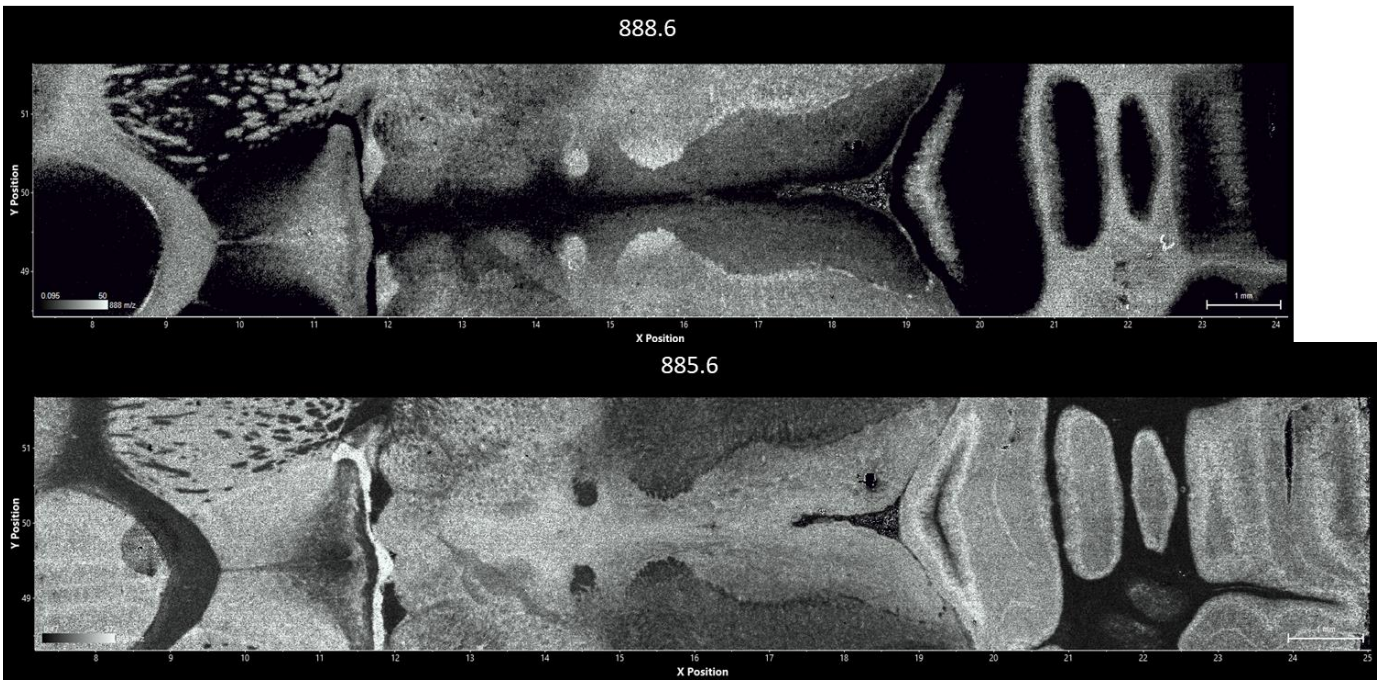


Figure 4 shows an expanded portion of 10 μm images of 885.6 (gray matter) and 888.6 (white matter) near the center of the segment.

In most respects the full images at 20 μm, 10 μm , and 5 μm spatial resolution are almost identical, but when expanded to show distribution of single pixels some small differences are found, For example at 10 μm resolution some pixels appear to correspond to single isolated cells. An example is illustrated in Figures 6, and 7. In the second expansion you can see the individual 10 μm pixels. Spectra from single pixels from the red and green areas are shown here. The vertical scale on these spectra is the number of ions detected in each bin of the digitizer. The total number of ions per peak obtained by integrating over the peak is typically about 3 times the peak intensity for these spectra. The number of ions detected in each peak is the value used in generating the 2D images. While many masses are common to both red and green pixels, the relative intensities of most are substantially different.

Optical image from on board camera

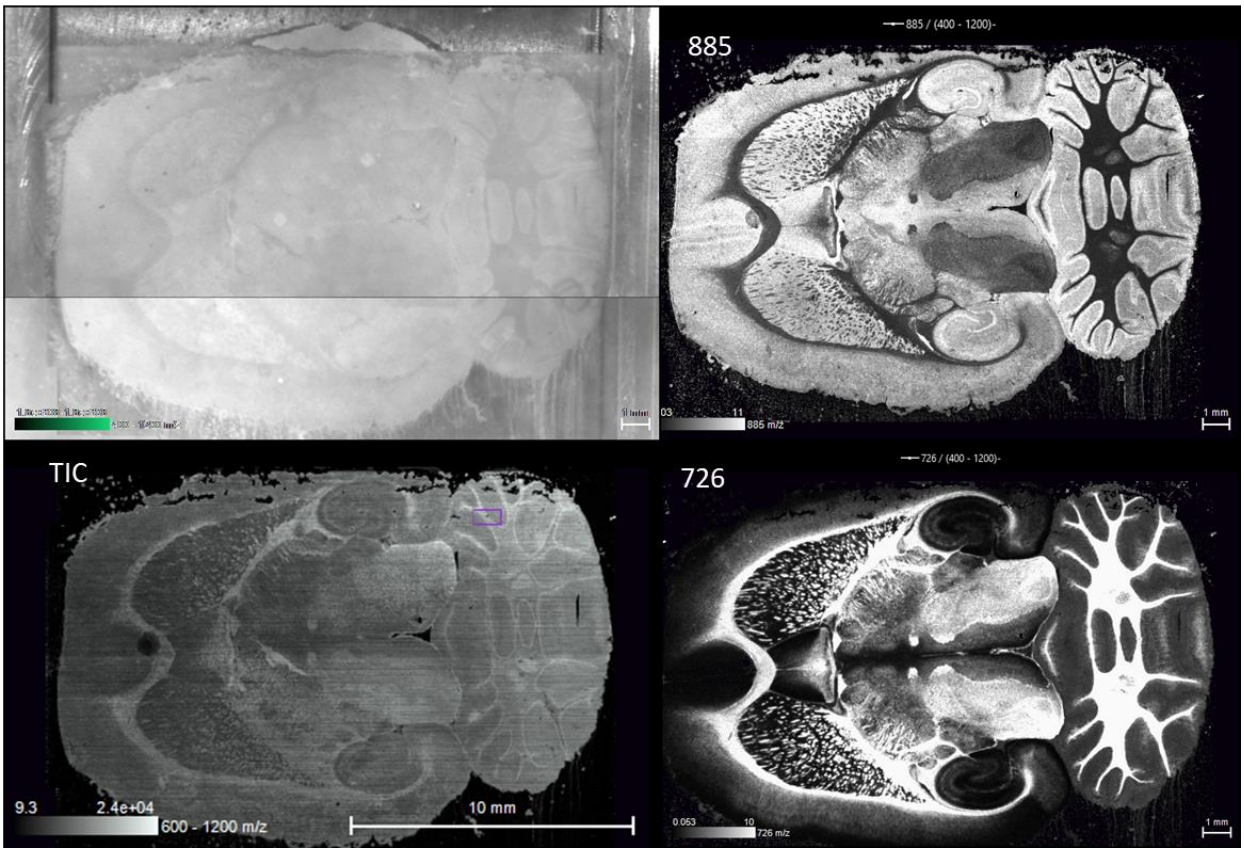


Figure 5 shows the optical image from the on-board camera in the upper left, TIC for m/z 600-1200 in lower left, with images for 885.6 and 726.6 in the right hand panels. 10 □m spatial Resolution, 5 kHz laser,10 shots/pixel, 5 mm/s scan,500 pixels/s acquired, 300 pixels/s saved, 3000 mass resolution, +/-0.1 Da mass accuracy.

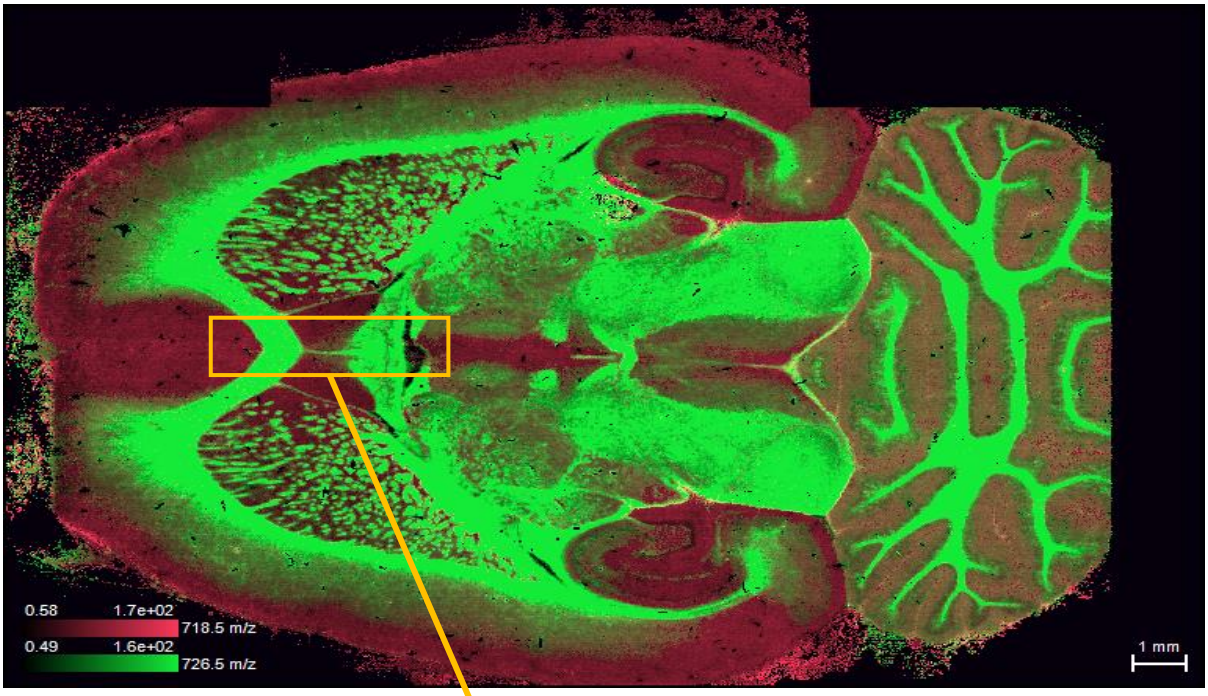


Figure 6 shows the image for m/z 726.5 in green and 718.5 in red. The region indicated in the yellow rectangle is expanded in Figure 7.

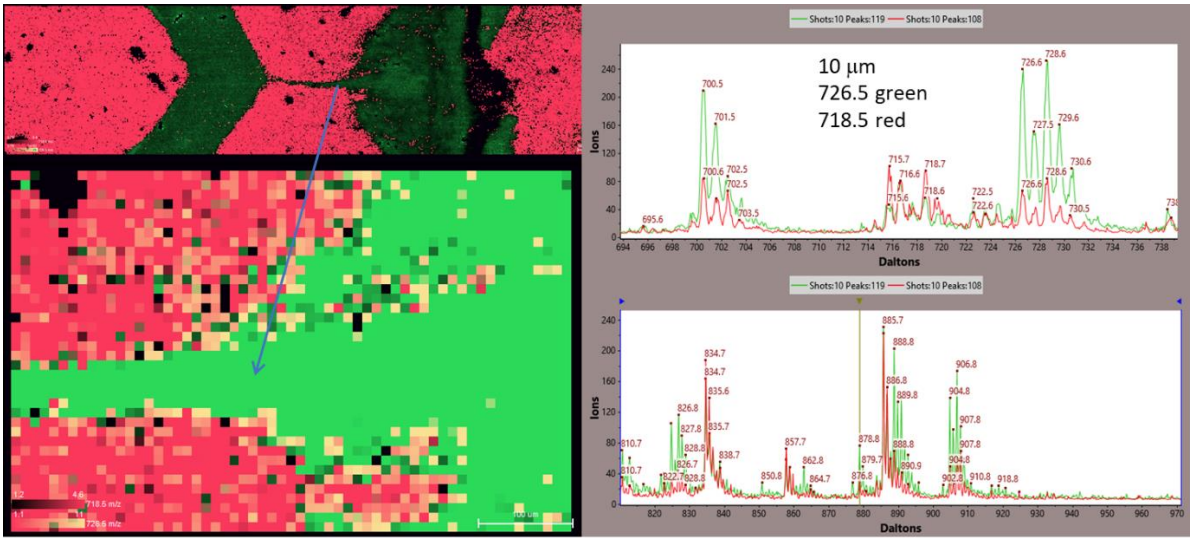


Figure 7 shows expansions of the region indicated in the yellow rectangle in Figure 6.

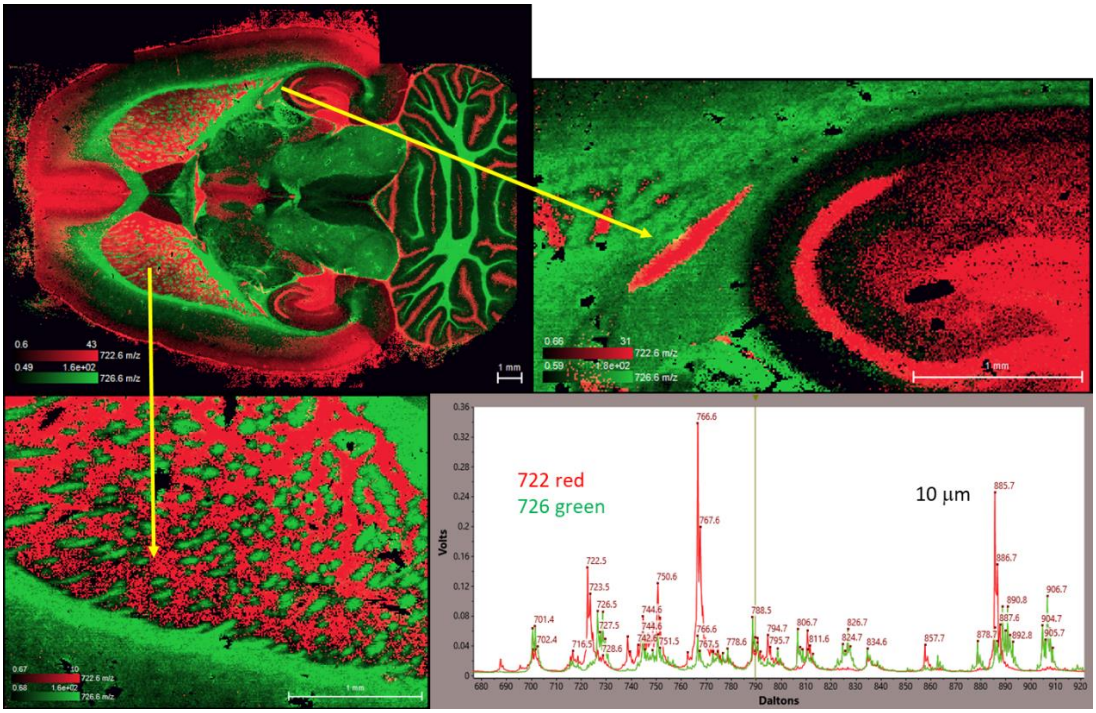


Figure 8 shows superimposed images of m/z 722 and 726 with expansions of two selected regions together with spectra obtained by averaging over small regions of the red and green. It should be noted that these masses are relatively small part of the TIC.

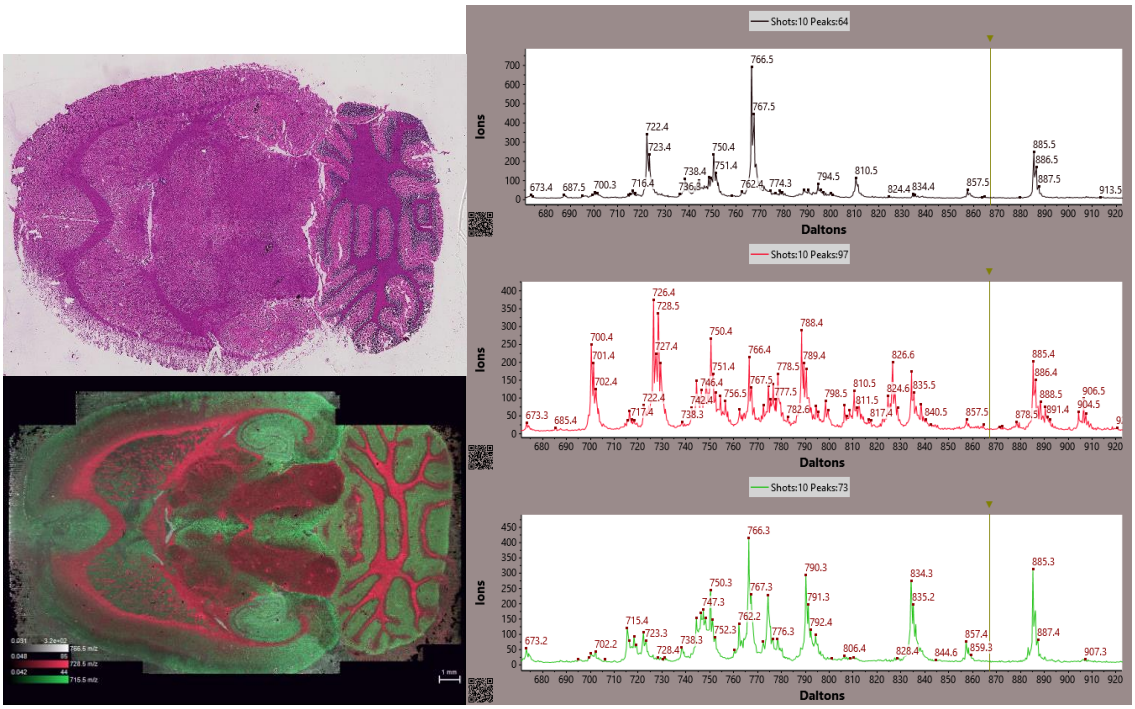


20 um m/z 715.5 green, 728.5 red, 766.5 white single pixels

Figure 9 shows images of m/z 715 (green), 728 (red), and 766 (white), with averaged spectrum from small selected regions of green, red, and white images. Spectra with high intensity of 885, 766, 750, and

722 appear to be lipid signatures of many cells on the surface. 766 is particularly intense in the small regions shown in white in the image.

These spectra are shown as the average intensity. This makes them independent of the number of pixels selected to provide the result. An H&E stain from one of the serial sections analyzed in this work is shown in the upper left panel of Figure 9. This is not the same section as imaged in Figure 9, but it is nearly the same and the correlation is obvious. In the future we will do an H&E stain on the actual sample and attempt to correlate the observed lipid profiles with the structures Ultimately the goal is to generate a 3-dimensional map of the lipid signatures for functional elements in an organ. These lipid signatures may then be applied to analysis of sections from controls and from purported disease state or trauma to provide a powerful tool for detection, diagnosis and treatment.

This ability to rapidly and accurately map lipid profiles in biological tissues has many important applications, since lipids are major structural components of biomembranes. Negatively charged species such as phosphatidylinositol, phosphatidylserine, sulfatides, and the zwitterionic phosphatidylethanolamines are major components of the cytoplasmic surface of the cellular membrane lipid bilayer and play a key role in several receptors signaling functions.[17 ] Lipids are not just involved in metabolic and neurological diseases; negatively charged lipids in particular play crucial roles in physiological events such as signal transduction, receptors, and enzymatic activation, as well as storage and release of therapeutic drugs and toxic chemicals in the body. Due to the importance of their role in signaling, the field of lipidomics has rapidly expanded in recent years.[19]

It is clear from our results that a specific negative ion lipid spectrum is generated for each pixel. Also many, but not all, pixels within a small area are essentially identical. The ultimate goal is to provide a method for generating a mass spectrometric signature for each cell, or collection of identical cells, in a tissue section. The present work has focused on negative ion spectra of lipids, but the method can be applied to other molecular signatures including positive ion spectra of lipids, peptides, proteins, and oligonucleotides.

**Conclusions and Future Work**

In evaluating this imaging instrument we employ the '7S' Criteria. Table I summarizes our results on these. As shown in the Table we have demonstrated high speed, high spatial resolution and wide dynamic range with lipids and other molecules with high surface concentrations, like the proteins and peptides in the islets of Langerhans.

Table I. Ideal Mass Spectrometer for MALDI MSI

- Satisfy the 7S-Criteria for performance
  - Speed – 300 pixels/s, 5kHz, 10 shots/pixel

| Spatial Resolution(μm) | Sample used(%) | min/cm$^2$ | pixels/cm$^2$ |
|---|---|---|---|
| 5 | 100 | 240 | 4,000,000 |
| 10 | 25 | 60 | 1,000,000 |
| 20 | 6 | 15 | 250,000 |

  - Trade-off between sensitivity, speed and size at lower spatial resolution (5 μm laser beam)

| Spatial Resolution(μm) | Sample used(%) | shots/pixel | pixel/s | min/cm$^2$ | pixels/cm$^2$ |
|---|---|---|---|---|---|
| 20 | 100 | 160 | 31.25 | 240 | 250,000 |
| 50 | 100 | 1000 | 5 | 240 | 40,000 |
| 100 | 100 | 4000 | 1.25 | 240 | 10,000 |

  - Survey scan prior to high spatial resolution (5 kHz, 5 mm/s)

| Spatial Resolution(μm) | Sample used(%) | shots/pixel | pixel/s | min/cm$^2$ | pixels/cm$^2$ |
|---|---|---|---|---|---|
| 50 | 10 | 50 | 100 | 6.7 | 40,000 |
| 100 | 5 | 100 | 50 | 3.4 | 10,000 |

  - Stability-1 billion laser shots since last cleaning 3 weeks ago
  - Simplicity-no tuning required

The observation in Figure 1 that the quality of the images are independent of the spatial resolution shows that the number of lipid ions detected per pixel with the 5 μm dia laser beam is independent of the spatial resolution. For molecules present at lower concentrations the sensitivity may be enhanced by rastering the 5 μm beam at 5 μm intervals and summing the results over a larger area. In this case there is a trade-off between speed and sensitivity according to the number of spectra summed/pixel. With the 5 μm laser beam the maximum time required to image a sample with area 1 cm$^2$ is 4 hours, but there is the obvious trade-off between sensitivity and spatial resolution. The other advantage of employing a laser beam with small diameter is that regions of interest can be found using a small fraction of the sample so that the rest can be used for higher spatial resolution or other analyses such as MS-MS

In carrying out the work on rat brain we used about 1 billion laser shots and there was no indication that the source needed to be cleaned. If the system is vented with dry gas, only about an hour of down time is required for cleaning. Other items that might require service are the laser and detector. We have not had enough failures to accurately determine lifetime of these, but we have run instruments for more than 100 billion laser shots with no problems. The instrument is fully automated and requires little expertise and training compared to sample prep and matrix application.

In conclusion, the linear MALDI-TOF instrument excels in all 7 criteria but specificity. High mass resolution MALDI-TOF and MS-MS instruments are required to provide elemental formula and structure of lipids imaged. Future work will focus on developing reflector MALDI-TOF and MS-MS systems that provide speed, spatial resolution, and sensitivity similar to that demonstrated here for the linear MALDI-TOF. The performance of this instrument shows that full 3D image of lipids is technically feasible with 10 μm spatial resolution for both positive and negative ions. Next step is to establish lipid signature for each cell detected in an image.

**Acknowledgements:** The authors are indebted to Katerina Djambazova, Jeff Spraggins, and Richard Caprioli from Vanderbilt University, not only for providing the samples used in this work, but also employing their extraordinary expertise in preparing the samples and applying the DAN matrix by sublimation.

**References**

1. Caprioli, RM, Farmer, TB, Gile, J. Molecular imaging of biological samples: localization of peptides and proteins using MALDI-TOF MS. Anal Chem. 1997; 69(23):4751–60.

2. Anderson, DMG, Spraggins, JM, Rose, KL, Schey, KKL. High spatial resolution imaging mass spectrometry of human optic nerve lipids and proteins. J. Am. Soc Mass Spectrom. 2015; 26(6):940-7.

3. Hamm, G, Porreaux, L, Stauber, J. Quantitative Mass Spectrometry Imaging (QMS) of endogenous insulin in mouse pancreas using modified insulin. Application Note #MSI-01. 2013. Imabiotech.

4. Ultra-high resolution MALDI-FTICR-MSI analysis of intact proteins in mouse and human pancreas tissue. Piga, I, Heijs, B, Nicolardi, S, Giusti, L, Marselli, L Marchetti, P, Mazzoni, MR, Lucacchini, A, McDonnellLA. Int J Mass Spectrom. 2017; 437(2019):10-16.

5. Barre, F, Rocha, B, Dewez, F, Towers, M, Murray, P, Claude, E, Cillero-Pastor, B, Heeren, R, Siegel, TP. Faster raster matrix-assisted laser desorption/ionization mass spectrometry imaging of lipids at high lateral resolution. Int. J. Mass Spectrom. 2018; 09:015.

6. Marvin Vestal, Lingjun Li, Evgenia Dobrinskikh, Yatao Shi, Bowen Wang, Xudong Shi, Sicheng Li, Christina Vestal, and Kenneth Parker; Fast MALDI-TOF Molecular Imaging: A Tale of Two Insulins as Told by Three Rats and Two Mice; BMS in press 2019 .

7. Marvin Vestal, Evgenia Dobrinskikh, Lingjun Li, Xiaoxin Wang, Christina Vestal, Sicheng Li, Kenneth Parker, Jeff Spraggins, and Richard Caprioli. Practical Method for Molecular Imaging with Single-Cell Resolution and Very High speed. MSACL 2018.

8. Vestal, M, Hayden, K. High performance MALDI-TOF mass spectrometry for proteomics; Int J Mass Spectrom. 2007; 268(2007):83-92.

9. Vestal, M. Modern MALDI time-of-flight mass spectrometry. J Mass Spectrom. 2009; 44(3):303-17.

10. Vestal, M. Evolution of quantitative MALDI-TOF mass spectrometry for clinical applications. Clin Chem. 2016; 62(1):20-3.

11. Yang, JH, Caprioli, RM. Matrix sublimation/recrystallization for imaging proteins by mass spectrometry at high spatial resolution. Anal Chem. 2011; 83(14):5728-34.

12. Deutskens, F,Yang, J, Caprioli, RM. High Spatial Resolution Imaging Mass Spectrometry and Classical Tissue Histology on a Single Tissue Section. J Mass Spectrom. 2011; 46:568-571.

13. Spraggins, JM, Caprioli, RM, J Am Soc Mass Spectrom. 2011; 22:1022-1031.

14. Schulz, Becker, Groseclose, Schadt, and Hopf; "Advanced MALDI mass spectrometry imaging in pharmaceutical research and drug development"; Current Opinion in Biotechnology 2019, 55:51-59.

15. Jansson, ET, Comi, TJ, Rubakhin, SS, Sweedler, JV. Single cell peptide heterogeneity of rat islets of Langerhans. ACS Chem Biol. 2016; 11(9):2588−95.

16. Jackson, SN, Wang, H-Y J, Woods, AS, Direct Profiling of Lipid Distribution in Brain Tissue Using MALDI-TOFMS. 2005; 77:4523-4527.

17. Jackson, SN, Wang, H-Y J, Woods, In Situ Characterization of Glycerophospholids and Sulfatides in Brain Tissue Using MALDI-MS/MS. J Am Soc Mass Spectrom. 2007; 18: 17-26.

18. Murphy, RC, Hankin, JA, Barkley, RM. Imaging of Lipid Species by MALDI mass spectrometry. J Lipid Res 2009; April Supplement S313-322.

19. Wenk, MR. Lipidomics: New Tools and Applications. Cell 2010; 888-894.